Inorganic Chemistry

Article

pubs.acs.org/IC

Alkaline Earth Metal (Mg, Sr, Ba)–Organic Frameworks Based on 2,2′,6,6′-Tetracarboxybiphenyl for Proton Conduction

Xi-Yan Dong,[†,‡] Xiao-Peng Hu,[†] Hong-Chang Yao,[†] Shuang-Quan Zang,*[,†] Hong-Wei Hou,[†] and Thomas C.W. Mak[†,§]

[†]College of Chemistry and Molecular Engineering, Zhengzhou University, Science Road No. 100, Zhengzhou 450001, China

[‡]School of Physics and Chemistry, Henan Polytechnic University, Jiaozuo 454000, China

[§]Department of Chemistry and Center of Novel Functional Molecules, The Chinese University of Hong Kong, Shatin, New Territories, Hong Kong SAR, China

Supporting Information

ABSTRACT: Three new alkaline earth metal based metal–organic frameworks (MOFs), namely **M-BPTC** (M = Mg, Sr, Ba), have been synthesized by using BPTC (2,2′,6,6′-tetracarboxybiphenyl) as ligand under hydrothermal conditions. These MOFs exhibit interesting structural diversity, variable chemical and thermal stability, as well as proton conductivity. **Mg-BPTC** with the formula $\{[Mg(BPTC)_{0.5}(H_2O)_3]\cdot 5H_2O\}_n$ consists of $BPTC^{4-}$ extended metal layers, and novel highly ordered infinite tape-like structures of cyclic water octamers reside interlayer. Three-dimensional porous $\{[Sr_2(BPTC)(H_2O)_6]\cdot H_2O\}_n$ (**Sr-BPTC**) features inorganic Sr–O chains (I^1O^2) and open hydrophilic channels where water heptamers and carboxyl oxygen atoms conspire to form H-bond networks, whereas 3D $\{[Ba_6(BPTC)_3(H_2O)_6]\cdot 11H_2O\}_n$ (**Ba-BPTC**) shows Ba–O inorganic layer (I^2O^1) and 1D channels incorporating large water 14-mers and 18-mers. **M-BPTC** (M = Mg, Sr) species exhibit excellent water stability and proton conductivity due to their respective appropriate pathways for proton transporting. **M-BPTC** (M = Sr, Ba) structures are highly thermally stable due to the presence of the inorganic connectivity. The present results suggest that **M-BPTC** (M = Mg, Sr) are promising materials for proton conduction and provide insight into the hydrogen bonding motif.

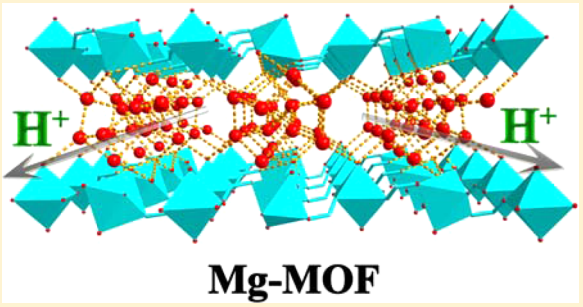

INTRODUCTION

Metal–organic frameworks (MOFs) have been an active research area in the past several years because of their potential applications across a broad range of technologies, i.e., gas storage, separation, catalysis, luminescence, ferroelectricity, and magnetism.[1] The proton conducting MOFs are new candidates for solid state proton (H^+) conductors potentially applied in fuel cells, hydrogen sensing, and electrochemical production of hydrogen, and therefore received attention recently.[2] Generally, 2D layered structures with hydrophilic interlayer and 3D porous frameworks containing open channels in MOFs are preferable candidates for proton conducting materials.[3] Also, the hydrogen bonded network formed by coordinated water, lattice water, and oxygen atoms of linkers (carboxylate, sulfonate, or phosphonate) in these pores is a favorable pathway for proton transfer.[2a,4] Moreover, water stability is of great importance for proton conducting materials, which usually operate in humid environment.[2b,5] Hitherto, it is still challenging to design water-stable MOFs with appropriate structure and pathways for proton conducting materials.

MOFs based on alkaline earth metals remain largely unexplored because of the inherent difficulties concerning the formation and crystallization of these MOFs.[6] However, alkaline earth ions have some unique advantages for application in materials science compared to other transition metals, such as being cheap and nontoxic.[6e] Additionally, many reported alkaline earth metal based MOFs with carboxylate ligands show high thermal stability, which is probably related to their relatively high charge density and ionic nature of these metal ions.[7] Especially, Sr^{2+} and Ba^{2+} have large ionic radii and hence possess a higher coordination number (6–10), which often leads to the resultant MOFs having inorganic connectivity and good thermal stability.[6a,7] It is mentioned that coordination polymers can be classified by considering their inorganic and organic connectivity, i.e., I^mO^n (m, n = 0, 1, 2, or 3). "I" refers to the dimensionality of the inorganic connectivity as embodied by metal–oxygen–metal (M–O–M) bonds, and "O" refers to the connectivity of the organic (ligand) component, i.e., M–ligand–M connectivity.[6a,7a,8] Thereby, MOFs assembled from alkaline earth metals attracted even more the attention of chemists and material scientists for their potential application in gas sorption, separation, and proton conducting materials.[9,10]

Biphenyl carboxylic acid ligands have been used to construct barium MOFs, which exhibit good thermal stability.[7a] H_4BPTC (2,2′,6,6′-tetracarboxybiphenyl) is a good linker for the construct

Received: July 22, 2014
Published: November 3, 2014

   dx.doi.org/10.1021/ic5017593 | Inorg. Chem. 2014, 53, 12050–12057

of intriguing MOFs due to the rich variety of coordination modes and the inherent flexibility.[11] Herein, we choose H_4BPTC and alkaline earth metal hydroxides to achieve well-characterized alkaline earth metal based MOFs, namely **M-BPTC** (M = Mg, Sr, Ba) for proton conduction, which are all synthesized with good yield and phase purity.

Layered **Mg-BPTC** incorporates novel highly ordered infinite water tapes consisting of fused cyclic water octamers and demonstrates water stability and proton conductivity of 2.6×10^{-4} S cm^{-1} at 100 °C and 98% relative humidity. For **Sr-BPTC**, Sr−O inorganic chains are connected by the linker BPTC^{4-} to form 3D porous structure (I^1O^2). Water heptamers in its hydrophilic channels are trapped in H-bonded network, which act as potential pathways for proton transfer. **Sr-BPTC** shows excellent water and thermal stability and proton conductivity of 2.7×10^{-4} S cm^{-1} at 90 °C and 98% relative humidity. Porous barium MOFs are rare in the literature.[7a,9b] **Ba-BPTC** demonstrates I^2O^1 connectivity, and the 2D inorganic layers constructed by Ba−O polyhedral are united by BPTC^{4-} linkers to generate 3D porous framework. Large water 14-mers and 18-mers are located in its 1D channel. **Ba-BPTC** demonstrates extraordinary air and thermal stability and maintains its crystallinity after the removal of guest water molecules.

EXPERIMENTAL SECTION

The literature method[12] was used for the preparation of H_4BPTC. Other starting materials were of reagent quality and were obtained from commercial sources without further purification.

Synthesis of [Mg(BPTC)$_{0.5}$(H$_2$O)$_3$]·5H$_2$O. Preparation was processed by reaction of $Mg(OH)_2{\cdot}4MgCO_3{\cdot}6H_2O$/$H_4$BPTC (0.8:1 mmol), in H_2O solution (4 mL) under hydrothermal conditions. The above mixture was stirred fully first and sealed in a 23 mL Teflon-lined stainless steel container, heated at 180 °C for 3 days and then cooled to room temperature. White single crystals of $[Mg_2(BPTC)_{0.5}(H_2O)_3]\cdot 5H_2O$ were isolated. Yield 90% (based on Mg). Anal. Calcd for **Mg-BPTC**: H 5.78, C 28.98. Found: H 5.41, C 28.78.

Synthesis of [Sr$_2$(BPTC)(H$_2$O)$_6$]·H$_2$O. The procedure is also similar to the synthesis of **Mg-BPTC** except that $Sr(OH)_2$ (0.5 mmol) was used instead of $Mg(OH)_2{\cdot}4MgCO_3{\cdot}6H_2O$. Yield 86% (based on Sr). Anal. Calcd for **Sr-BPTC**: H 3.21, C 30.62. Found: H 3.01, C 30.48.

Synthesis of [Ba$_6$(BPTC)$_3$(H$_2$O)$_6$]·11H$_2$O. The procedure is also similar to the synthesis of **Mg-BPTC** except that $Ba(OH)_2$ (0.5 mmol) was used instead of $Mg(OH)_2{\cdot}4MgCO_3{\cdot}6H_2O$. Yield 83% (based on Ba). Anal. Calcd for **Ba-BPTC**: H 2.37, C 27.69. Found: H 2.15, C 27.48.

Water Treatment and Activation. The crystals of **M-BPTC** (M = Mg, Sr, Ba) are immersed in water for one month, and then filtered and dried in air to obtain the water-treated samples. The dehydrated phase of **M-BPTC** (M = Sr, Ba) is obtained via evacuation under vacuum at 90 °C for 24 h. Water vapor adsorption measurements were performed using the activated samples of **Sr-BPTC**.

Physical Measurements. X-ray single-crystal diffraction data were collected on a Bruker SMART1000 CCD diffractometer with Mo Kα radiation (λ = 0.710 73 Å) at room temperature. The empirical absorption corrections were applied by using the SADABS program.[13] Fourier transform (FT) IR spectra (KBr pellet) (Supporting Information Figure S5) were recorded at room temperature on a PerkinElmer FT-IR spectrometer. Powder X-ray diffraction patterns were recorded on a Phillips XPERT PRO with Cu Kα irradiation (λ = 1.5418 Å). TGA measurement was performed on a PE Diamond TG/DTA unit under air atmosphere at a rate of 10 °C min^{-1} in the temperature range 25−800 °C. Proton conductivity was measured on the powdered crystalline samples **M-BPTC** (M = Mg, Sr) in tablets under a pressure of 220 M Pa. Alternating current impedance spectroscopy measurement was performed on a PARSTAT 2273 impedance analyzer over a frequency range from 0.1 Hz to 1 MHz, with a quasi-four-probe electrochemical cell and an applied ac voltage of 10 mV with copper electrodes (the purity of Cu is more than 99.9%). The measurements were conducted at room temperature 23 °C and different relative humidity (RH), as well as at RH = 98% and different temperature.

Crystal Structure Determination. Single-crystal X-ray diffraction data of complexes **M-BPTC** (M = Mg, Sr, Ba) were collected on a Bruker SMART APEX CCD diffractometer equipped with graphite monochromatized Mo Kα radiation (λ = 0.710 73 Å) at room temperature using the ω-scan technique. Empirical absorption corrections were applied to the intensities using the SADABS program.[13] The structures were solved using the program SHELXS-97[14] and refined with the program SHELXL-97.[15] All nonhydrogen atoms were subjected to anisotropic refinement. The hydrogen atoms of the organic ligands were included in the structure factor calculation at idealized positions using a riding model and refined isotropically. The hydrogen atoms of the coordinated and solvent water molecules were located from difference Fourier maps, and then restrained at fixed positions and refined isotropically. There is Alert B in the checkcif file reporting D−H without acceptor. This is because a large number of water molecules in these compounds, in which H atoms of water molecules are difficult to assign the exact position from the SCXRD. Also, the involved water molecules have been associated with other O atoms through hydrogen bonds. The crystallographic data and selected bond distances and angles for **M-BPTC** (M = Mg, Sr, Ba) are listed in Table 1 and Tables S1−S3 in the Supporting Information, respectively.

Table 1. Crystal Data and Structure Refinement for M-BPTC (M = Mg, Sr, Ba)

	Mg-BPTC	Sr-BPTC	Ba-BPTC
T	293 K	293 K	293 K
formula	$C_8H_{19}MgO_{12}$	$C_{16}H_{20}Sr_2O_{15}$	$C_{96}H_{98}Ba_{12}O_{79}$
fw	331.54	627.56	4163.82
cryst syst	monoclinic	monoclinic	monoclinic
space group	$C2/c$	$P2_1/c$	$P2_1/c$
Z	8	4	2
a (Å)	19.020(2),	13.6876(6)	19.4778(2)
b (Å)	7.7962(9)	10.4272(6)	13.9542(1)
c (Å)	19.565(2)	15.0005(7)	23.761(2)
α	90.000	90.00	90.00
β	92.355	100.256(4)	104.444(2)
γ	90.000	90.00	90.00
V (Å^3)	2898.7(6)	2106.71(2)	6253.9(1)
ρ_{calcd} (g cm^{-3})	1.519	1.978	2.211
θ range (deg)	2.99−25.00	2.96−25.00	1.08−25.00
F(000)	1400	1248	3956
μ (cm^{-1})	0.182	5.142	3.823
reflns collected	5687	8434	33 405
indep reflns	2523	3714	11 018
completeness	98.8%	99.8%	100%
R(int)	0.0482	0.071	0.0440
GOF	0.988	1.009	1.027
R1^a [$I > 2\sigma(I)$], wR2^b	0.0982, 0.2469	0.0522, 0.1003	0.0328, 0.0959
R1^a [all data], wR2^b	0.1197, 0.2603	0.0786, 0.1103	0.0449, 0.1025

^{a}R1 = $\sum||F_o| - |F_c||/\sum|F_o|$. ^{b}wR2 = $[\sum w(F_o^2 - F_c^2)^2/\sum w(F_o^2)^2]^{1/2}$.

CCDC-1007250 (**Mg-BPTC**), CCDC-1007251 (**Sr-BPTC**), and CCDC-1007252 (**Ba-BPTC**) contain the supplementary crystallographic data for this Article. These data can be obtained free of charge from The Cambridge Crystallographic Data Centre via www.ccdc.cam.ac.uk/data_request/cif.

RESULTS AND DISCUSSION

Crystal Structure of Mg-BPTC. **Mg-BPTC** crystallizes in $C2/c$ space group (Table 1) and is constructed from a layer substructure (Figure 1a). As shown in Supporting Information

dx.doi.org/10.1021/ic5017593 | Inorg. Chem. 2014, 53, 12050−12057

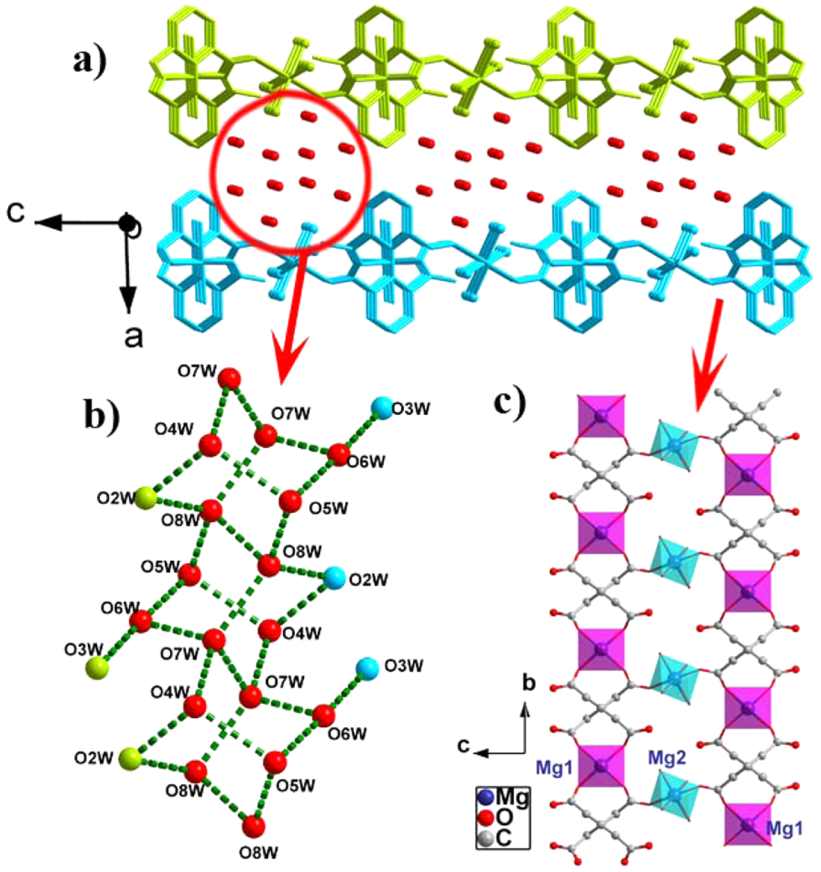

Figure 1. (a) View of **Mg-BPTC** with 1D channels located between interlay; H atoms are omitted for clarity. (b) Hydrogen bonding association of water molecules into extended tapes with dangling water molecules. Color codes: lattice water (red); coordinated water molecules above and below the plane (green and blue). (c) Polyhedral representation for a single layer structure constructed by $BPTC^{4-}$ and Mg^{2+}.

Table 2. Hydrogen Bond Separation between Water Oxygen Atoms (Å) of the Water Tape in Mg-BPTC, Water Heptamer in Sr-BPTC, and Water 14-Mer and 18-Mer in Ba-BPTC

		Water Tape in **Mg-BPTC**			
O2W···O8W	2.829(1)	O8W···O5W	2.784(8)	O4W···O5W	2.917(4)
O7W···O4W	2.829(2)	O8W···O7W	2.784(8)	O2W···O4W	2.949(1)
O5W···O6W	2.834(2)	O8W···O8W	2.800(8)	O3W···O6W	3.042(4)
O6W···O7W	2.834(6)	O7W···O7W	2.827(8)		
		Water Heptamer in **Sr-BPTC**			
O3W···O6W	2.714(4)	O3W···O7W	2.823(0)	O1W···O7W	2.872(9)
O5W···O7W	2.931(0)	O5W···O6W	3.024(0)	O2W···O3W	3.068(4)
O6W···O4W	3.124(2)	O6W···O4W	3.124(2)		
		Water 14-Mer in **Ba-BPTC**			
O12W···O13W	2.621(9)	O1W···O10W	2.805(3)	O13W···O15W	2.883(3)
O12W···O15W	2.896(1)	O7W···O10W	2.907(2)	O1W···O12W	2.930(6)
O3W···O15W	3.012(3)				
		Water 18-Mer in **Ba-BPTC**			
O16W···O17W	2.674(5)	O11W···O14W	2.732(5)	O8W···O14W	2.773(6)
O5W···O16W	2.792(8)	O14W···O17W	2.856(6)	O8W···O17W	2.864(7)
O4W···O5W	2.915(6)	O8W···O9W	2.920(9)	O9W···O11W	3.055(0)
O6W···O17W	3.147(8)				

Figure S1, the asymmetric unit of **Mg-BPTC** contains two Mg atoms (Mg1 and Mg2 having an occupancy of 0.5), half $BPTC^{4-}$ ligand, three coordinated water molecules, and five free water molecules. Selected bond lengths and angles are listed in Supporting Information Table S1. In the asymmetry unit, two Mg^{2+} cations possess distorted octahedral geometry to give MgO_6 octahedra with the bond length of Mg−O from 2.03(7) to 2.11(1) Å, which is comparable with another Mg carboxylate complex.[9] Mg1 is hexacoordinated to four oxygen atoms from two $BPTC^{4-}$ anions, and two coordinated water molecules to give MgO_6 octahedra. Mg2 is ligated by two oxygen atoms from two different $BPTC^{4-}$ anions, and four coordinated water molecules. The carboxylate groups of $BPTC^{4-}$ anion display bidentate (μ_2-η^1,η^1) and bidentate chelate coordination modes.

dx.doi.org/10.1021/ic5017593 | *Inorg. Chem.* 2014, 53, 12050−12057

Each $BPTC^{4-}$ anion serves as a μ_4-bridge to coordinate four Mg ions (Supporting Information Figure S4). Mg1 and $BPTC^{4-}$ ligand form one-dimensional chain, with a dihedral angle of 73.02° between the two benzene rings, which are further connected by Mg2 to generate a layer motif. The interlayer separation is about 5.50 Å.

Notably, **Mg-BPTC** reveals interlayer hydrophilic 1D channels running parallel to the *b* axis, which are filled with lattice and coordinated waters. The hydrogen bonding association leads to the formation of an novel water tape T5(3)5(3)5(2)5(2)A1 along the *b* axis (Figure 1b).[16] This water tape consists of novel water octamer with the geometry of noncoplanar cyclic structure in the sequence O2W−O8W−O8W−O5W−O6W−O7W−O7W−O4W. The water octamer is composed of four basic cyclic five-membered rings and an eight-membered ring. Adjacent octamers are fused together by sharing one edge formed by O8W···O8W with the separation of 2.801 Å, forming a one-dimensional water tape along the *b* axis. Additional O3W water molecules are bonded to O6W at the vertex of the octamer to decorate the tapes. The O···O distances vary from 2.785 to 3.042 Å with an average O···O separation of 2.858 Å, compared to 2.85 Å in liquid water.[17] The data presented in Table 2 also suggest the hydrogen bonding interaction among the water molecules. Such highly ordered infinite water tapes consisting of fused cyclic water octamers have not been reported previously and are a potential proton conducting pathway.

Crystal Structure of Sr-BPTC. **Sr-BPTC** is a 3D porous structure (Figure 2a) and crystallizes in the $P2_1/c$ space group (Table 1). As shown in Supporting Information Figure S2, the asymmetric unit of **Sr-BPTC** contains two Sr atoms, one $BPTC^{4-}$ ligand, six coordinated water molecules, and one free water molecule. Selected bond lengths and angles are listed in Supporting Information Table S2, which shows that the Sr−O bond lengths range from 2.538 to 2.920 Å. This larger range of bond lengths has also been seen in another Sr coordination polymer.[9] Both eight-coordinated Sr1 and nine-coordinated Sr2 are ligated by five carboxyl group oxygen atoms, and three and four water molecules occur in the coordination sphere of Sr1 and Sr2, respectively. In the asymmetric unit, Sr1 and Sr2 share the edge composed of O2#1 and O8. The adjacent two Sr2 share the plane composed of O3, O3#, O1W, and O1W#. The adjacent two Sr1 share the edge composed of O1#1 and O1#3. Sr−O inorganic connectivity results in 1D inorganic chains which are further connected by the μ_6-BPTC ligands in two directions to generate the 3D framework of **Sr-BPTC** (Figure 2b), so **Sr-BPTC** can be classified as I^1O^2 connectivity. The $BPTC^{4-}$ anion displays tetradentate (μ_4-η^2,η^2), tridentate (μ_3-η^1,η^2), bidentate (μ_2-η^2,η^0), and monodentate coordination fashions and serves as a μ_6-bridge to coordinate six Sr ions, with a dihedral angle of 66.04° between the two benzene rings (Supporting Information Figure S4). The extremely hydrophilic porous channels were constructed along the *c*-axis having a cross-section of approximately 9.4 × 9.7 $Å^2$.

Coordinated water molecules (O1W, O2W, O3W, O4W, O5W, O6W) located at the hydrophilic channel wall and free water molecule (O7W) are assembled into a heptamer, whose core is a cyclic tetramer (O3W, O5W, O6W, O7W) in the distorted quadrilateral conformation with O···O distances in the range 2.71−3.01 Å (Table 2, Figure 2c). The remaining three water molecules are attached above and below the distorted quadrilateral. It is important that Sr-ligated water molecules, free water, and carboxyl oxygen atoms are connected into the H-bonding network, which is favorable for proton transfer (Figure 2d).[2a,4]

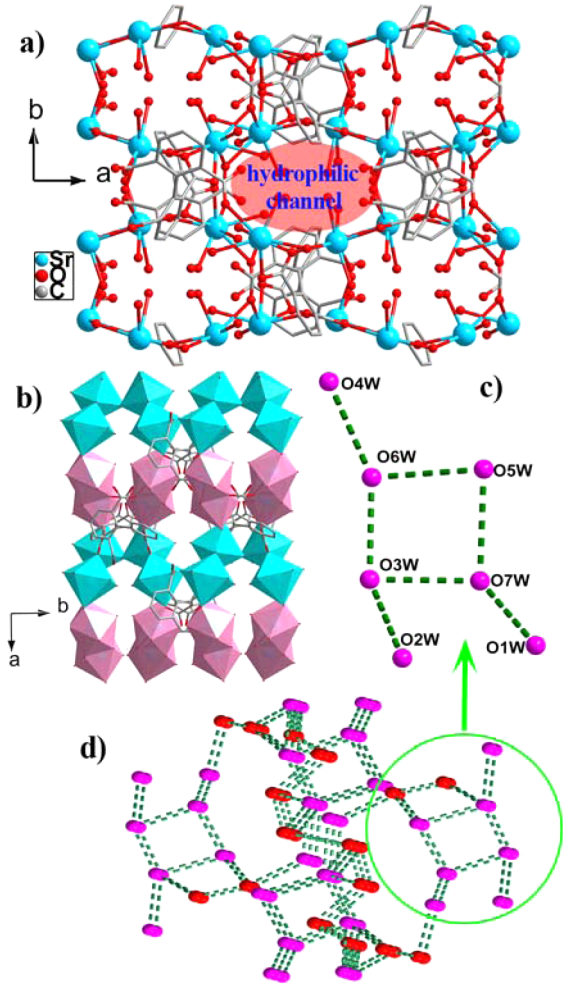

Figure 2. (a) Crystal structure of **Sr-BPTC**, H atoms are omitted for clarity. (b) Polyhedral representation of Sr−O inorganic chains which are united by $BPTC^{4-}$ to form 3D structure. (c) Water heptamer composed of coordinated and noncoordinated water molecules in the hydrophilic channels. (d) H-bonded networks composed of water molecules (pink) and carboxyl oxygen atoms (red).

Crystal Structure of Ba-BPTC. **Ba-BPTC** exhibits 3D open framework (Figure 3a) with I^2O^1 connectivity and also crystallizes in $P2_1/c$ space group (Table 1). As shown in Supporting Information Figure S3, the asymmetric unit of **Ba-BPTC** contains 6 Ba atoms, 3 $BPTC^{4-}$ ligands (designed as BPTC-1, BPTC-2, BPTC-3, respectively), 6 coordinated water molecules, and 11 free water molecules. Selected bond lengths and angles are listed in Supporting Information Table S3. The coordination modes of $BPTC^{4-}$ in this case are very rich and mainly exhibit tetradentate (μ_4-η^2,η^2), tridentate (μ_3-η^1,η^2), and bidentate (μ_2-η^1,η^1) coordination modes (Supporting Information Figure S4). The BPTC-1, with a dihedral angle of 68.73° between the two benzene rings, serves as a μ_6-bridge to coordinate six Ba ions. The BPTC-2 with a dihedral angle of 69.25° between the two benzene rings acts as μ_8-bridge linker to coordinate eight Ba ions. The BPTC-3, with a dihedral angle of 66.43° between the two benzene rings, serves as a μ_7-bridge to ligate seven Ba ions. Six barium ions have different coordination numbers, viz., 7, 8, and 9. The Ba−O bond lengths ranging from 2.650 to 3.056 Å are in accordance with those previously

dx.doi.org/10.1021/ic5017593 | *Inorg. Chem.* 2014, 53, 12050−12057

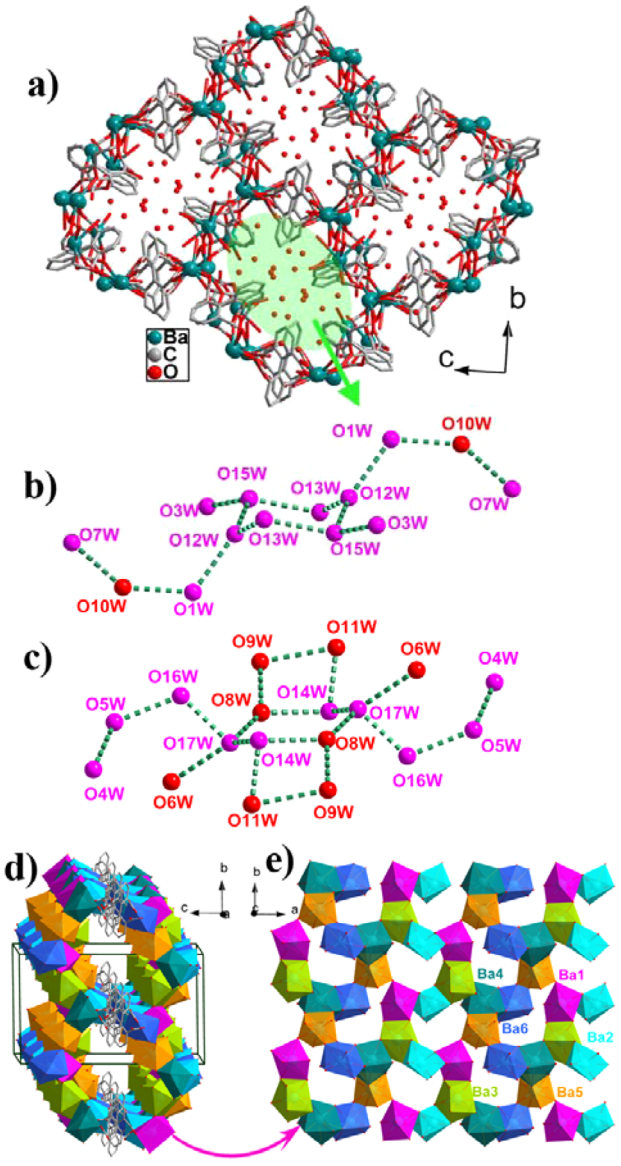

Figure 3. (a) View of 3D **Ba-BPTC** structure with 1D channels along *a* axis, H atoms are omitted for clarity. (b) Water 14-mer. (c) Water 18-mer. Color code: magneta, free water; red, aqua ligand. (d) Ba−O inorganic layer are connected $BPTC^{4-}$ to form three-dimensional net in **Ba-BPTC**. (e) Polyhedral representation of Ba−O inorganic layer.

reported.[6,7,9b] Ba1 ions (Ba_1O_7) are coordinated to seven O atoms, with six of them from the carboxylate groups of the $BPTC^{4-}$ ligand and one coordinated water molecule. Ba2 ions are coordinated to eight O atoms (Ba_2O_8), including six carboxylate oxygen atoms and two water oxygen atoms, sharing the edge composed of O1 and O13 with Ba1 polyhedron. Ba3 ions are coordinated to nine O atoms, five belonging to carboxyl groups and four from coordinated water molecules. Also, Ba_3O_9 polyhedron shares the edge composed of O10 and O24 with Ba_1O_7 polyhydron. Nine-coordinated Ba4 and Ba6 ions are ligated to seven carboxyl O atoms and two coordinated water molecules, leading to Ba_4O_9 and Ba_6O_9 ployhedron. Ba_5O_9 polyhedron contains three coordinated water molecules and six oxygen atoms from $BPTC^{4-}$. These Ba−O polyhedra are connected by face-sharing, edge-sharing, and top-sharing to form 2-D wave inorganic layer structure (Figure 3e), which are further connected by $BPTC^{4-}$ to form 3D framework and surround 1D channels along the *a* axis (Figure 3d). Thus, **Ba-BPTC** can be classified as I^2O^1 connectivity. The dimension of the channel is estimated as 6.8 × 12.8 $Å^2$. Such inorganic connectivity usually makes the compound possess good thermal stability.[6a,7,9b]

Two discrete water clusters (water 14-mer and 18-mer) are found in the channels. In the small 14-mer (Figure 3b), the cyclic hexamer of chair conformation is formed by free water molecules (O12W, O13W, O15W) and their symmetry-related counterparts, with O3W monomer and H-bounded O1W−O10W−O7W string dangling from O15W and O12W, respcetively. The O···O distances in the cyclic hexamer fall in the range 2.622−3.012 Å with an average O···O separation of 2.865 Å, compared to 2.85 Å in liquid water.[17]

The conformation of water 18-mer (Figure 3c) also includes chairlike hexamer core, which is composed of coordinated water (O8W) and free water (O14W, O17W) as well as their counterparts. The two identical four-membered rings share an edge with the hexamer core. Coordinated monomer O6W and water string O16W−O5W−O4W via H-bond association are dangling from O17W. The hydrogen bonded O···O distances vary from 2.674 to 3.148 Å with an average of O···O separation of 2.752 Å (Table 2), which is shorter than that (2.865 Å) in the water 14-mer and compared to 2.74 Å in ice I_c or 2.76 in ice I_h.[18]

Thermal and Water Stability Studies. The phase purity of the bulk sample was confirmed by matching the powder X-ray diffraction (PXRD) pattern of these compounds **M-BPTC** (M = Mg, Sr, Ba) and the PXRD pattern simulated from single crystal analysis (Figure 4). Thermal analyses in air of complexes **M-BPTC** (M = Mg, Sr, Ba) have revealed that their backbone decomposed up to 510, 547, 543 °C, respectively, with the observed water weight loss of 41.04%, 19.98%, 14.29% (calculated 43.43%, 20.07%, 14.51%), respectively. The dehydrated phase of **Mg-BPTC** loses its crystallinity although its backbone decomposed up to 510 °C. This is probably because the loss of interlay water molecules results in the collapse of the layered structure, whereas the evacuated **M-BPTC** (M = Sr, Ba) samples can retain the original porous framework (Figure 5). The good thermal stability of **M-BPTC** (M = Sr, Ba) may be attributed to their inorganic connectivity and the ionic nature of bonds between Sr^{2+} and Ba^{2+} and negative charge ions, which have no preferable binding direction. Such a type of coordination sphere is flexible and highly thermally stable.

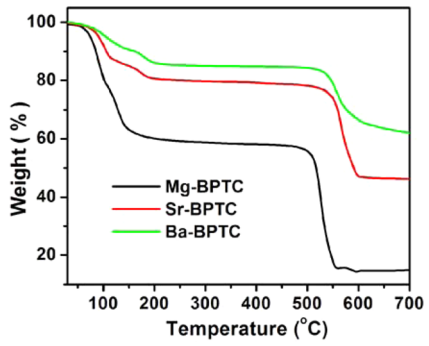

Figure 4. Thermogravimetric analyses of the as-synthesized **M-BPTC** (M = Mg, Sr, Ba) in air.

To determine the stability of the compounds toward water, these compounds were immersed in water over one month, and the PXRD pattern was recorded upon drying. The PXRD patterns of as-synthesized and water-treated **M-BPTC** (M = Mg,

dx.doi.org/10.1021/ic5017593 | *Inorg. Chem.* 2014, 53, 12050−12057

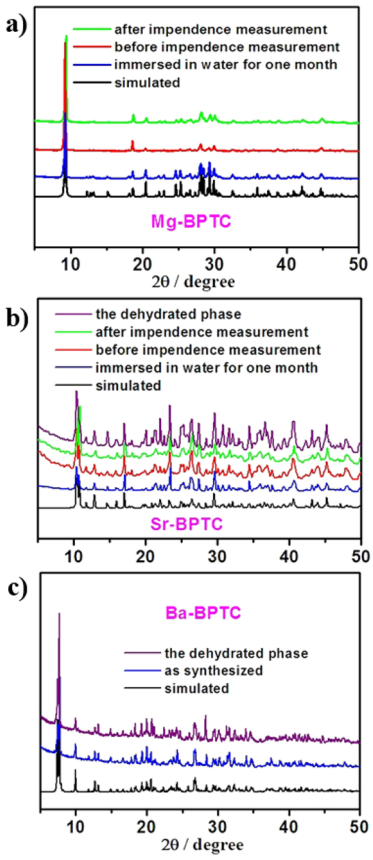

Figure 5. Powder XRD patterns of **M-BPTC** (M = Mg, Sr, Ba): the simulated patterns according to single crystal structural determinations; the as-synthesized crystals, the water treated crystals, the dehydrated phase, the compressed pellet before impendence measurement and after impendence measurement.

Sr) samples overlapped well. Furthermore, the structures of **M-BPTC** (M = Mg, Sr) were maintained even after long-time impedance measurements (Figure 5) (as discussed below). These above results confirmed the excellent stability of **M-BPTC** (M = Mg, Sr) toward water. However, phase transition occurred for **Ba-BPTC** after long-time immersion in water at room temperature, though it has a 2D inorganic connectivity layer with high thermal stability. For **M-BPTC** (M = Mg, Sr), the high water content and excellent water stability offer excellent opportunities as proton conducting materials.

Proton Conductive Properties. Considering the structure and the water stability, the impedance ($Z^* = Z' + iZ''$) of complex **M-BPTC** (M = Mg, Sr) pellet was measured as a function of relative humidity (RH) at room temperature and as a function of temperature at RH = 98%. The overall resistance (R) of the polycrystalline samples was obtained from arc extrapolation to the Z' axis on the low frequency side of the Nyquist plot. The corresponding conductivity (σ) was calculated taking into account the thickness (d) and flat surface area (A) of the pellet: $\sigma = d/(RA)$. The plots of $\log(\sigma T)$ versus $1000/T$ are linear and can be fitted to the equation $T\sigma = \sigma_0 \exp(-E_a/kT)$, where σ_0 is a pre-exponential factor and E_a, k, and T are the apparent activation energy for conduction, Boltzmann's constant, and the absolute temperature, respectively. In each case, the activation energy for ionic transport was determined by measuring the ionic conductivity at various temperatures.

For **Mg-BPTC**, Nyquist plots are shown in Figure 6. In the Nyquist plots, the frequency response of the pellet consists of

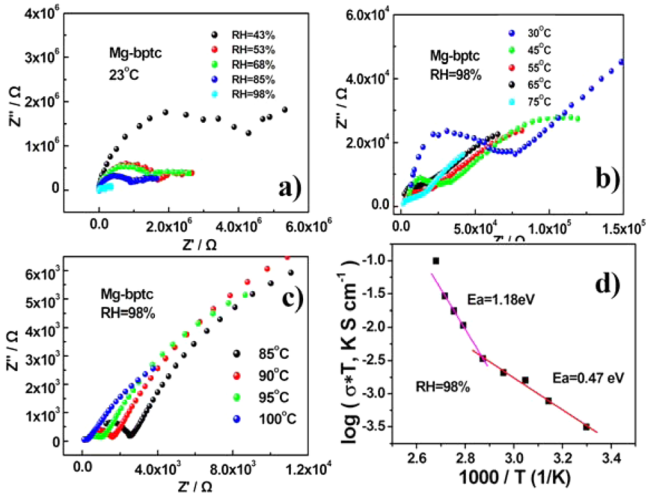

Figure 6. Impedance spectra of **Mg-BPTC**: (a) at 23 °C and different RH, (b) from 30 to 75 °C at 98% RH, (c) from 85 to 90 °C at 98% RH, (d) Arrhenius plots of the proton conductivities of **Mg-BPTC** at 98% RH.

one semicircle and a spur due to the response of the electrode–pellet interface appears in these plots. The conductivity of the pellet changes from 1.8×10^{-8} to 6.9×10^{-7} S cm^{-1} when relative humidity increases from 43% to 98% at 23 °C. Proton conductivity is dependent on the temperature and reached 2.6×10^{-4} S cm^{-1} at 100 °C and 98% RH (Supporting Information Table S4), which is moderate compared with that of other proton conducting coordination polymer under the same tested conditions (Supporting Information Table S6). The activation energies in the ranges 30–65 and 65–100 °C are 0.47 and 1.18 eV, respectively. The activation energy (E_a) of proton conductivity below 65 °C for **Mg-BPTC** was estimated to be 0.47 eV, which is relatively high compared with that of typical hydrated proton conductors, which conduct through a Grotthuss mechanism, such as Nafion. Yet, some proton conducting materials have been reported to possess E_a slightly higher than 0.40 eV, where the Grotthuss mechanism is likely to occur.[2a,19] For **Mg-BPTC**, the metal cations serve to enhance the acidity of the water molecules (O1W, O2W, O3W), which can donate protons to adjacent lattice water molecules;[20] thereby, proton transport proceeds in well-defined hydrogen bonding networks (Supporting Information Figure S6). Meanwhile, the above process may be concomitant with partially direct diffusion of additional protons with water molecules (the vehicle mechanism) in the interlayer space.[19a] Whereas, above 65 °C, the free water in interlayer space combined with the absorbed water may get mobile between the layers, which could transport protons over long ranges resulting in the high ion conductivity and a high activation of 1.18 eV.[21] This changeable proton conductive mechanism between low temperature and high temperature has also been observed in other proton conducting materials.[22]

Nyquist plots of **Sr-BPTC** are shown in Figure 7. It is observed that the conductivity increases as the humidity increases and attains 1.6×10^{-6} S cm^{-1} at RH = 98% at 23 °C. The temperature dependence of proton conductivity over the temperature range 30–100 °C at 98% RH was measured (Supporting Information Table S5), which increased with temperature, reached a maximum of 2.7×10^{-4} S cm^{-1} at 90 °C, and then slightly

dx.doi.org/10.1021/ic5017593 | Inorg. Chem. 2014, 53, 12050–12057

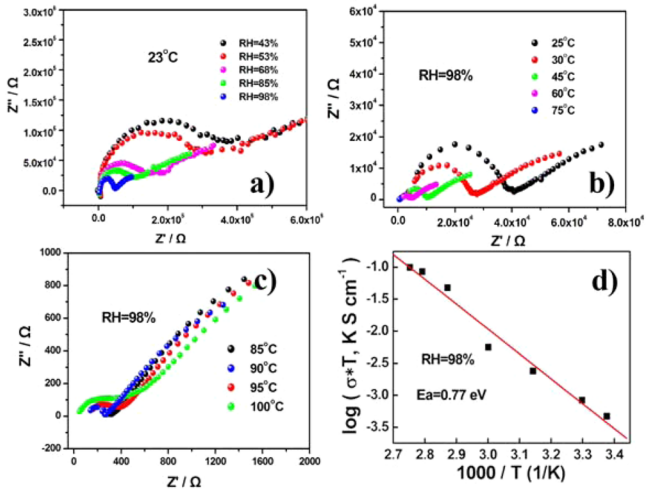

Figure 7. Impedance spectra of **Sr-BPTC**: (a) at 23 °C and different RH, (b) from 25 to 75 °C at 98% RH, (c) from 85 to 100 °C at 98% RH, (d) Arrhenius plot of the proton conductivities of **Sr-BPTC**.

decreased but remained on the order of 10^{-4} S cm^{-1} until 100 °C, which is the same order of magnitude with that of **Mg-BPTC** at the same conditions. The slight decrease of proton conductivity above 90 °C may be attributed to desorption of water molecules even at 98% RH. The data before 90 °C are fitted to the Arrhenius expression to give activation energy (E_a) of 0.77 eV at 98% RH. Since the dehydrated **Sr-BPTC** retains the original structure, the water vapor adsorption and desorption were measured to understand the relationship between the humidity and conducting behavior. As shown in Supporting Information Figure S7, the dehydrated **Sr-BPTC** exhibited a large amount of water vapor adsorption in the low-pressure region. At about a relative pressure (P/P_0) of 0.1, the amount of adsorption arrived at about 5 water molecules per asymmetric unit, reflecting that water molecules are easily captured by metal ion Sr^{2+} with open coordination sites in the dehydrated phase. At RH 85%, the water vapor uptake is almost 6 water molecules, which corresponds to the number of coordinated water molecules on Sr. After that, rapid capillary condensation occurs, and the number of water molecules is up to a value of 12 at maximum humidity. The extra adsorbed water molecules are located around aqua ligands acidified by metal ions and could accept protons from them to form hydronium ions, with their corporate migration along the hydrophilic channels resulting in proton transport via vehicle mechanism.[21] The possible pathway of proton migration in **Sr-BPTC** is proposed and depicted in Supporting Information Figure S8. Although both **Mg-BPTC** and **Sr-BPTC** include highly coordinated water as proton donor and efficient hydrogen bond associated water-mediated pathways, there is a difference in the proton transport mechanism, which may be related to their inherent structure.

Taken together, these above results suggested that both 1D channels and 2D layers incorporating H-bond networks are the appropriate pathways for proton conduction. Coordinated waters can play an important role in supplying proton carriers. Cheap and nontoxic alkaline earth (AE) metals may be alternative candidates for proton conducting MOFs with good chemical and thermal stability.

CONCLUSIONS

We have successfully synthesized three new MOFs using alkaline earth metal hydroxides. They exhibit interesting structural diversity, variable chemical stability, thermal stability, as well as proton conduction. Most interestingly, novel water structures are incorporated in these MOFs, such as 1D infinite rare water tape in **Mg-BPTC**, water heptamer **Sr-BPTC**, and water 14-mer and 18-mer in **Ba-BPTC**. **Mg-BPTC** and **Sr-BPTC** are water-stable and demonstrate high proton conductivity because of their respective appropriate pathways for proton transporting. These results may motivate researchers to explore new alkaline earth metal based MOFs, materials for proton conduction. The present finding may also provide insight into the hydrogen bonding motif of the aqueous environment and help unravel the mechanism of proton transfer in proton conducting materials.

ASSOCIATED CONTENT

Supporting Information

Crystal structure of **M-BPTC** (M = Mg, Sr, Ba), IR spectrum, proton conductivity, water adsorption, X-ray crystallographic files (CIF), and analysis on the impedance plots. This material is available free of charge via the Internet at http://pubs.acs.org.

AUTHOR INFORMATION

Corresponding Author

*E-mail: zangsqzg@zzu.edu.cn.

Notes

The authors declare no competing financial interest.

ACKNOWLEDGMENTS

This work was supported by the National Natural Science Foundation of China (No. 21371153, 20901070), Program for Science & Technology Innovation Talents in Universities of Henan Province (13HASTIT008), and Key Scientific and Technological Project of Henan Province (132102210411) and Zhengzhou University.

REFERENCES

(1) Special issues on MOFs: (a) *Chem. Rev.* **2012**, *112*, 673−1268. (b) *Chem. Soc. Rev.* **2009**, *38*, 1201−1508.

(2) (a) Ramaswamy, P.; Wong, N. E.; Shimizu, G. K. H. *Chem. Soc. Rev.* **2014**, *43*, 5913−5932. (b) Yamada, T.; Otsubo; Makiura, K. R.; Kitagawa, H. *Chem. Soc. Rev.* **2013**, *42*, 6655−6669. (c) Yoon, M.; Suh, K.; Natarajan, S.; Kim, K. *Angew. Chem., Int. Ed.* **2013**, *52*, 2688−2700. (d) Horike, S.; Umeyama, D.; Kitagawa, S. *Acc. Chem. Res.* **2013**, *46*, 2376−2384. (e) Xu, G.; Otsubo, K.; Yamada, T.; Sakaida, S.; Kitagawa, H. *J. Am. Chem. Soc.* **2013**, *135*, 7438−7441. (f) Colodrero, R. M. P.; Papathanasiou, K. E.; Stavgianoudaki, N.; Olivera-Pastor, P.; Losilla, E. R.; Aranda, M. A. G.; León-Reina, L.; Sanz, J.; Sobrados, I.; Choquesillo-Lazarte, D.; García-Ruiz, J. M.; Atienzar, P.; Rey, F.; Demadis, K. D.; Cabeza, A. *Chem. Mater.* **2012**, *24*, 3780−3792.

(3) (a) Sadakiyo, M.; Yamada, T.; Honda, K.; Matsui, H.; Kitagawa, H. *J. Am. Chem. Soc.* **2014**, *136*, 7701−7707. (b) Ōkawa, H.; Sadakiyo, M.; Yamada, T.; Maesato, M.; Ohba, M.; Kitagawa, H. *J. Am. Chem. Soc.* **2013**, *135*, 2256−2262. (c) Wei, M.-L.; Wang, X. X.; Duan, X. Y. *Chem.—Eur. J.* **2013**, *19*, 1607−1616. (d) Chen, W.-X.; Xu, H.-R.; Zhuang, G.-L.; Long, L.-S.; Huang, R.-B.; Zheng, L.-S. *Chem. Commun.* **2011**, *47*, 11933−11935. (e) Taylor, J. M.; Mah, R. K.; Moudrakovski, I. L.; Ratcliffe, C. I.; Vaidhyanathan, R.; Shimizu, G. K. H. *J. Am. Chem. Soc.* **2010**, *132*, 14055−14057.

(4) (a) Sadakiyo, M.; Yamada, T.; Honda, K.; Matsui, H.; Kitagawa, H. *J. Am. Chem. Soc.* **2014**, *136*, 7701−7707. (b) Pardo, E.; Train, C.; Gontard, G.; Boubekeur, K.; Fabelo, O.; Liu, H.; Dkhil, B.; Lloret, F.; Nakagawa, K.; Tokoro, H.; Ohkoshi, S.; Verdaguer, M. *J. Am. Chem. Soc.*

2011, *133*, 15328−15331. (c) Ohkoshi, S.; Nakagawa, K.; Tomono, K.; Imoto, K.; Tsunobuchi, Y.; Tokoro, H. *J. Am. Chem. Soc.* **2010**, *132*, 6620−6621.
(5) (a) Mauritz, K. A.; Moore, R. B. *Chem. Rev.* **2004**, *104*, 4535−4585. (b) Alberti, G.; Casciola, M. *Solid State Ionics* **2001**, *145*, 3−16.
(6) (a) Chen, X.; Plonka, A. M.; Banerjee, D.; Parise, J. B. *Cryst. Growth Des.* **2013**, *13*, 326−332. (b) Plonka, A. M.; Banerjee, D.; Parise, J. B. *Cryst. Growth Des.* **2012**, *12*, 2460−2467. (c) Foo, M. L.; Horike, S.; Inubushi, Y.; Kitagawa, S. *Angew. Chem., Int. Ed.* **2012**, *51*, 6107−6111. (d) Platero-Prats, A. E.; Iglesias, M.; Snejko, N.; Monge, Á.; Gutiérrez-Puebla, E. *Cryst. Growth Des.* **2011**, *11*, 1750−1758. (e) Banerjee, D.; Parise, J. B. *Cryst. Growth Des.* **2011**, *11*, 4704−4720.
(7) (a) Chen, X.; He, S.; Chen, F.; Feng, Y. *CrystEngComm* **2014**, *16*, 8706−8709. (b) Foo, M. L.; Horike, S.; Duan, J.; Chen, W.; Kitagawa, S. *Cryst. Growth Des.* **2013**, *13*, 2965−2972. (c) Yeh, C.-T.; Lin, W.-C.; Lo, S.-H.; Kao, C.-C.; Lin, C.-H.; Yang, C.-C. *CrystEngComm* **2012**, *14*, 1219−1222.
(8) Cheetham, A. K.; Rao, C. N. R.; Feller, R. K. *Chem. Commun.* **2006**, 4780−4795.
(9) (a) Rankine, D.; Keene, T. D.; Sumby, C. J.; Doonan, C. J. *CrystEngComm* **2013**, *15*, 9722−9728. (b) McDonald, T. M.; Lee, W. R.; Mason, J. A.; Wiers, B. M.; Hong, C. S.; Long, J. R. *J. Am. Chem. Soc.* **2012**, *134*, 7056−7065. (c) Jayaramulu, K.; Narayanan, R. P.; George, S. J.; Maji, T. K. *Inorg. Chem.* **2012**, *51*, 10089−10091. (d) Banerjee, D.; Zhang, Z.; Plonka, A. M.; Li, J.; Parise, J. B. *Cryst. Growth Des.* **2012**, *12*, 2162−2165. (e) Foo, M. L.; Horike, S.; Kitagawa, S. *Inorg. Chem.* **2011**, *50*, 11853−11855. (f) Caskey, S. R.; Wong-Foy, A. G.; Matzger, A. J. *J. Am. Chem. Soc.* **2008**, *130*, 10870−10871. (g) Rood, J. A.; Noll, B. C.; Henderson, K. W. *Inorg. Chem.* **2006**, *45*, 5521−5528.
(10) (a) Bazaga-García, M.; Colodrero, R. M. P.; Papadaki, M.; Garczarek, P.; Zoń, J.; Olivera-Pastor, P.; Losilla, E. R.; León-Reina, L.; Aranda, M. A. G.; Choquesillo-Lazarte, D.; Demadis, K. D.; Cabeza, A. *J. Am. Chem. Soc.* **2014**, *136*, 5731−5739. (b) Horike, S.; Kamitsubo, Y.; Inukai, M.; Fukushima, T.; Umeyama, D.; Itakura, T.; Kitagawa, S. *J. Am. Chem. Soc.* **2013**, *135*, 4612−4615. (c) Liang, X.; Zhang, F.; Feng, W.; Zou, X.; Zhao, C.; Na, H.; Liu, C.; Suna, F.; Zhu, G. *Chem. Sci.* **2013**, *4*, 983−992. (d) Kundu, T.; Sahoo, S. C.; Banerjee, R. *Chem. Commun.* **2012**, *48*, 4998−5000. (e) Mallick, A.; Kundu, T.; Banerjee, R. *Chem. Commun.* **2012**, *48*, 8829−8831. (f) Wiers, B. M.; Foo, M.-L.; Balsara, N. P.; Long, J. R. *J. Am. Chem. Soc.* **2011**, *133*, 14522−14525.
(11) (a) Li, B.; Zang, S.-Q.; Ji, C.; Hou, H.-W.; Mak, T. C. W. *Cryst. Growth Des.* **2012**, *12*, 1443−1451. (b) Chang, Z.; Zhang, D.-S.; Chen, Q.; Li, R.-F.; Hu, T.-L.; Bu, X.-H. *Inorg. Chem.* **2011**, *50*, 7555−7562. (c) Huang, Y.-G.; Gong, Y.-Q.; Jiang, F.-L.; Yuan, D.-Q.; Wu, M.-Y.; Gao, Q.; Wei, W.; Hong, M.-C. *Cryst. Growth Des.* **2007**, *7*, 1385−1387. (d) Suh, M. P.; Moon, H. R.; Lee, E. Y.; Jang, S. Y. *J. Am. Chem. Soc.* **2006**, *128*, 4710−4718.
(12) Pryor, K. E.; Shipps, G. W., Jr.; Skyler, D. A.; Rebek, J., Jr. *Tetrahedron* **1998**, *54*, 4107−4124.
(13) Sheldrick, G. M. *SADABS 2.05*; University of Göttingen: Germany.
(14) (a) Sheldrick, G. M. *Acta Crystallogr., Sect. A* **1990**, *46*, 457. (b) Sheldrick, G. M. *SHELXS-97, Program for Solution of Crystal Structures*; University of Göttingen: Germany, 1997.
(15) Sheldrick, G. M. *SHELXL-97, Program for Crystal Structures Refinement*; University of Göttingen: Germany, 1997.
(16) (a) Han, L.-L.; Hu, T.-P.; Chen, J.-S.; Li, Z.-H.; Wang, X.-P.; Zhao, Y.-Q.; Li, X.-Y.; Sun, D. *Dalton Trans.* **2014**, *43*, 8774−8780. (b) Infantes, L.; Chisholm, J.; Motherwell, S. *CrystEngComm* **2003**, *5*, 480−486. (c) Infantes, L.; Motherwell, S. *CrystEngComm* **2002**, *4*, 454−461.
(17) (a) Ma, B.-Q.; Sun, H.-L.; Gao, S. *Chem. Commun.* **2004**, 2220−2221. (b) Liu, K.; Brown, M. G.; Cruzan, J. D.; Saykally, R. J. *Science* **1996**, *271*, 62−64. (c) Narten, A. H.; Thiessen, W. E.; Blum, L. *Science* **1982**, *217*, 1033−1034.
(18) (a) Eisenberg, K. D.; Kauzmann, W. *The Structure and Properties of Water*; Oxford University Press: Oxford, 1969. (b) Zhao, H.-X.; Kong, X.-J.; Li, H.; Jin, Y.-C.; Long, L.-S.; Zeng, X.-C.; Huang, R.-B.; Zheng, L.-S. *Proc. Natl. Acad. Sci. U.S.A.* **2011**, *108*, 3481−3486. (c) Zhang, Z.-H.; Chen, S.-C.; He, M.-Y.; Li, C.; Chen, Q.; Du, M. *Cryst. Growth Des.* **2011**, *11*, 5171−5175.
(19) (a) Sadakiyo, M.; Yamada, T.; Kitagawa, H. *J. Am. Chem. Soc.* **2014**, *136*, 13166−13169. (b) Inukai, M.; Horike, S.; Chen, W.; Umeyama, D.; Itakura, T.; Kitagawa, S. *J. Mater. Chem. A* **2014**, *2*, 10404−10409. (c) Umeyama, D.; Horike, S.; Inukai, M.; Itakura, T.; Kitagawa, S. *J. Am. Chem. Soc.* **2012**, *134*, 12780−12785. (d) Colodrero, R. M. P.; Olivera-Pastor, P.; Losilla, E. R.; Hernández-Alonso, D.; Aranda, M. A. G.; Leon-Reina, L.; Rius, J.; Demadis, K. D.; Moreau, B.; Villemin, D.; Palomino, M.; Rey, F.; Cabeza, A. *Inorg. Chem.* **2012**, *51*, 7689−7698. (e) Sadakiyo, M.; Yamada, T.; Kitagawa, H. *J. Am. Chem. Soc.* **2009**, *131*, 9906−9907. (f) Kreuer, K. D. *Chem. Mater.* **1996**, *8*, 610−641.
(20) (a) Jeong, N. C.; Samanta, B.; Lee, C. Y.; Farha, O. K.; Hupp, J. T. *J. Am. Chem. Soc.* **2012**, *134*, 51−54. (b) Taylor, J. M.; Mah, R. K.; Moudrakovski, I. L.; Ratcliffe, C. I.; Vaidhyanathan, R.; Shimizu, G. K. H. *J. Am. Chem. Soc.* **2010**, *132*, 14055−14057.
(21) (a) Bhattacharya, S.; Gnanavel, M.; Bhattacharyya, A. J.; Natarajan, S. *Cryst. Growth Des.* **2014**, *14*, 310−325. (b) Dong, X.-Y.; Wang, R.; Li, J.-B.; Zang, S.-Q.; Hou, H.-W.; Mak, T. C. W. *Chem. Commun.* **2013**, *49*, 10590−10592. (c) Wei, M.-L.; Wang, J.-H.; Wang, Y.-X. *J. Solid State Chem.* **2013**, *198*, 323−329. (d) Kreuer, K.-D.; Rabenau, A.; Weppner, W. *Angew. Chem., Int. Ed. Engl.* **1982**, *21*, 208−209.
(22) Hurd, J. A.; Vaidhyanathan, R.; Thangadurai, V.; Ratcliffe, C. I.; Moudrakovski, I. L.; Shimizu, G. K. H. *Nat. Chem.* **2009**, *1*, 705−710.